Electronic Supplementary Material (ESI) for RSC Chemical Biology.

SUPPORTING INFORMATION

The two domains of human galectin-8 bind sialyl- and fucose-containing oligosaccharides in an independent manner. A 3D view by using NMR

NMR EXPERIMENTS

General information

The total volume for all NMR samples employed in this study was 500 µL, analyzed within a precision NMR tube with 5 mm outer diameter (New Era Enterprises, Vineland, USA). The pH of all buffers was measured with a Crison Basic 20 (Crison Instruments SA, Barcelona, Spain) pH-meter and carefully adjusted with the suitable amount of NaOH and HCl or NaOD and DCl.

Saturation Transfer Difference (STD) NMR

All STD experiments were acquired using Bruker AVANCE 2 800 MHz spectrometer equipped with cryoprobe. The STD spectra acquired for ligands **1**, **3** and **6** are reported here, as well as a visual representation of the epitope map and the relative STD-AF intensities for each irradiation.

Interaction of ligands 1, 3 and 6 with Gal-8FL.

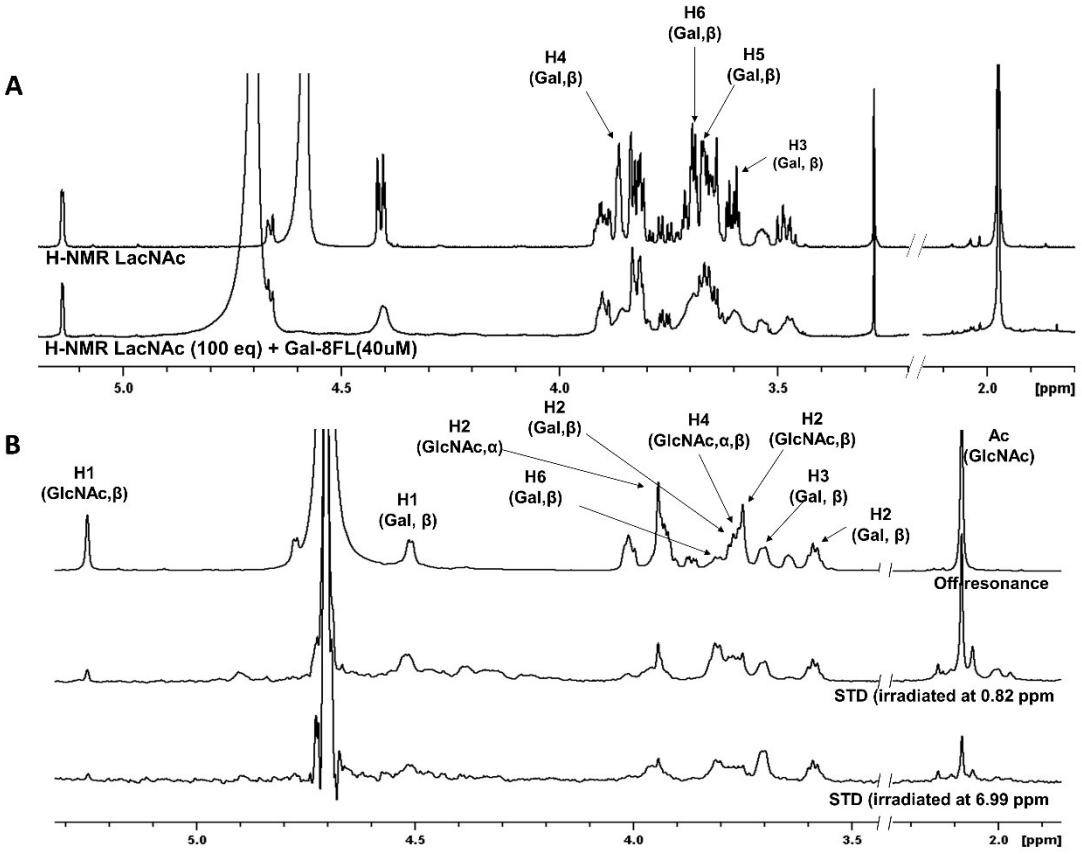

C

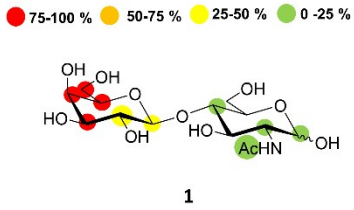

1

Residue	Atom	STD-AF (Aliphatics, 0.61 ppm)	STD (%) (Aliphatics)	STD-AF (Aromatics, 6.99 ppm)	STD (%) (Aromatics)
GlcNAcα	H1	0.0022	7.2	0.0006	6.5
	H2	0.0046	15.0	0.0013	14.1
	H4	0.0077	25.2	0.0017	18.5
	Ac	0.0073	23.8	0.0012	13.0
GlcNAcβ	H2	0.0046	15.0	0.0012	13.0
	H4	0.0077	25.2	0.0017	18.5
	Ac	0.0073	23.8	0.0012	13.0
Galβ	H1	0.0097	31.7	0.0027	29.3
	H2	0.0091	29.7	0.0040	43.5
	H3	0.0091	29.7	0.0070	76.1
	H4	0.0022	70.9	0.0092	100
	H5	0.0108	35.3	0.0021	22.8
	H6	0.0306	100	0.0075	81.5

Fig S1. Binding epitope of LacNAc (**1**) determined by signal broadening on ^{1}H-NMR and ^{1}H-STD-NMR. **A**) Above: 1H-NMR spectra of ligand **1** alone; below: ^{1}H-NMR spectra of *h*Gal-8FL and LacNAc (the sample contained 40 µM of *h*Gal-8FL, with aratio lectin:**1** = 1:100. Signal broadening was clearly identified for H3-H6 protons of β-Gal unit. **B**) ^{1}H-STD-NMR spectra. Above: Off-resonance spectrum (irradiation at -30 ppm). The signals showing STD intensity were indicated; below: STD spectra (irradiation at 0.82 ppm and at 6.99 ppm). **C**) Visual depiction of the epitope mapping for the *h*Gal-8FL:LacNAc (**1**) interaction including the relative STD-AF intensities and STD percentage based on the most intense STD signals.

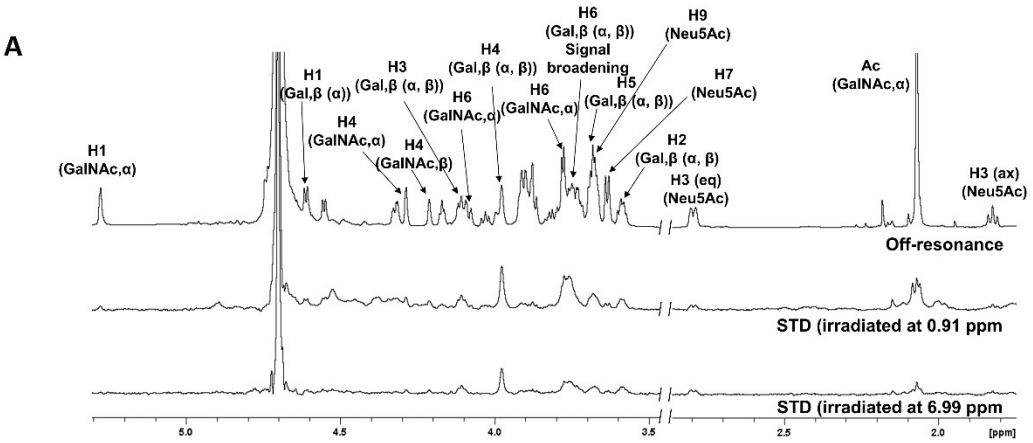

B

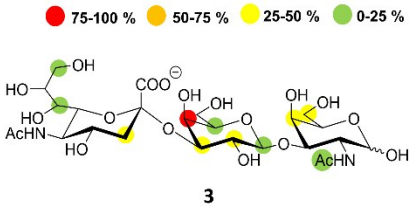

3

Residue	Atom	STD-AF (Aliphatics, 0.61 ppm)	STD (%) (Aliphatics)	STD-AF (Aromatics, 6.99 ppm)	STD (%) (Aromatics)
GalNAcα	H1	0.0035	11.4	-	-
	H3	0.0076	24.8	-	-
	H4	0.0098	32.0	0.0030	16.1
	H6	0.0128	41.8	0.0048	25.8
	H6'	0.0107	35.0	0.0028	15.0
	Ac	0.0035	11.4	-	-
GalNAcβ	H3	0.0036	11.8	0.0012	6.4
	H4	0.0101	33.0	0.0040	21.5
Galβ (α)*	H1	0.006	19.6	-	-
	H2	0.0115	37.6	0.0079	42.5
	H3	0.0134	43.8	0.0078	41.9
	H4	0.0306	100	0.0186	100
	H5	0.0062	20.3	0.0023	12.4
Galβ (β)	H1	0.0104	34.0	-	-
	H2	0.0115	37.6	0.0079	42.5
	H3	0.0134	43.8	0.0078	41.9
	H4	0.0306	100	0.0186	100
	H5	0.0062	20.3	0.0023	12.4
Neu5Ac	H3 (ax)	0.0096	31.4	0.0066	35.5
	H3 (eq)	0.0074	24.2	0.0066	35.5
	H7	0.0039	12.7	0.0020	10.7
	H9	0.0037	12.1	0.0017	9.1

*Galβ (α) and Galβ (β) refer to the fact that the presence of GalNAcα and GalNAcβ induces the presence of two different signals for some protons of Galβ.

Fig S2. A) ^{1}H-STD-NMR for *h*Gal-8 and 3-Sialyl-Galβ1-3GalNAc (**3**). The sample contained *h*Gal-8FL 30 µM and ligand **3** in 0.9 mM (ratio lectin:ligand = 1:30). **A**) Above: Off-resonance spectrum (irradiation at -30 ppm) and above: STD spectra (irradiation in the aliphatic region at 0.91 ppm and irradiation in the aromatic region at 6.99 ppm). **B**) Visual depiction of the epitope mapping for the *h*Gal-8FL : 3-Sialyl--Galβ1-3GalNAc (**3**) interaction including the relative STD-AF intensities and STD percentage based on the most intense STD signals.

A

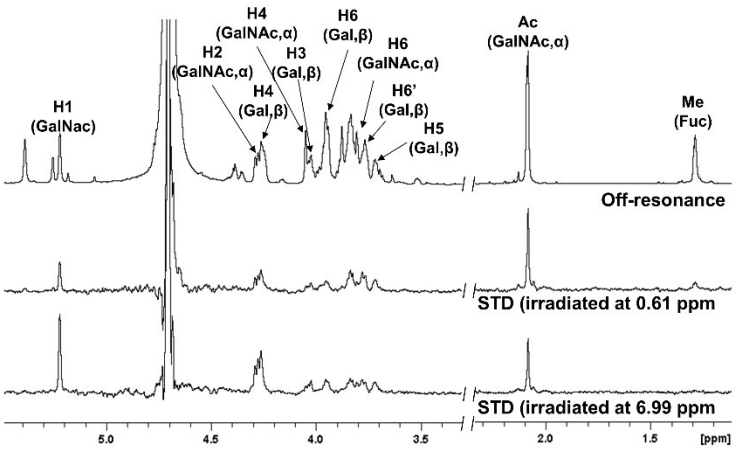

B

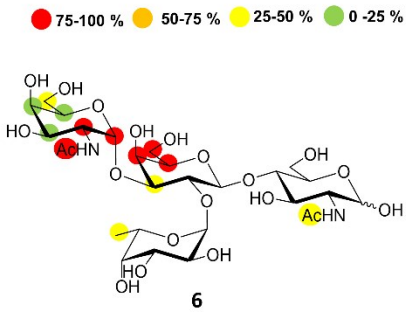

Residue	Atom	STD-AF (Aliphatics, 0.61 ppm)	STD (%) (Aliphatics)	STD-AF (Aromatics, 6.99 ppm)	STD (%) (Aromatics)
GlcNAc	Ac	0.003	33.7	0.0054	7.6
Galβ	H3	0.0042	47.2	0.0226	31.9
	H4	0.0071	79.8	0.0474	66.9
	H5	0.0071	79. 8	0.0226	31.9
	H6	0.0089	100	0.0219	30.9
	H6'	0.0045	50.6	0.0097	13.7
GalNAcα	H1	0.0079	88.7	0.0708	100
	H2	0.0074	83.1	0.0536	75.7
	H4	0.0016	18.0	0.0064	9.03
	H6	0.0024	27.0	0.0094	13.3
	Ac	0.0089	100	0.0216	30.5
Fuc	CH3	0.0024	27.0	-	-

Fig S3. ^{1}H-STD-NMR for *h*Gal-8 and A type II (**6**). The sample contained *h*Gal-8FL 40 µM, **6** 1.2 mM (ratio lectin:ligand = 1:30). **A**) Above: Off-resonance spectrum (irradiation at -30 ppm) and below: STD spectra (irradiation in the aliphatic region at 0.61 ppm and irradiation in the aromatic region at 6.99 ppm). **B**) Visual depiction of the epitope mapping for the *h*Gal-8FL : A type II interaction including the relative STD-AF intensities and STD percentage based on the most intense STD signals.

Interaction of ligands 3 and 6 with Gal-8N and Gal-8C.

For comparison purposes ^{1}H-STD NMR experiments of ligands 3 and 6 with Gal-8N and Gal-8C, respectively, were acquired and the results are included in Fig S4-S5.

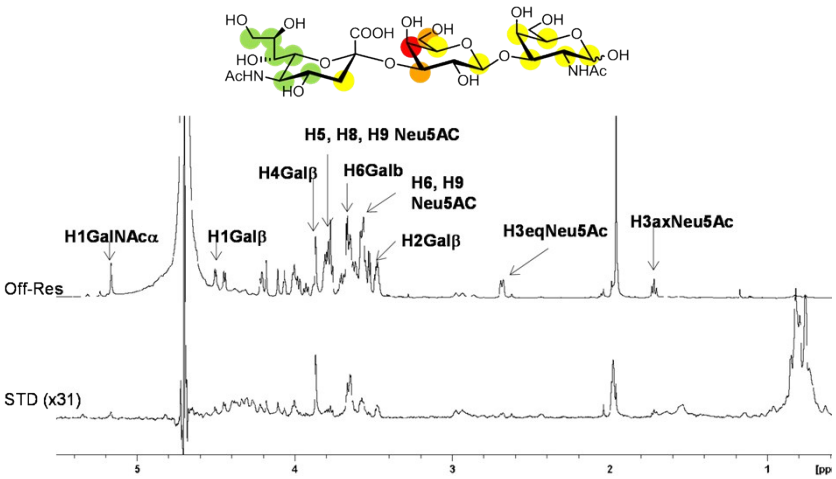

Fig S4. ^{1}H-STD-NMR experiment recorded at 298K for Gal-8N and 3-Sialyl-Galβ1-3GalNAc (**3**). The sample contained Gal-8N 50 µM and ligand **3** in 1.0 mM (ratio lectin:ligand = 1:20). **A**) Above: Determined epitope mapping for 3-Sialyl-Galβ1-3GalNAc (**3**). Below: Off-resonance (irradiation at -30 ppm) and STD spectra (irradiation in the aliphatic region at 0.73 ppm) indicating the signals with the highest STD intensities.

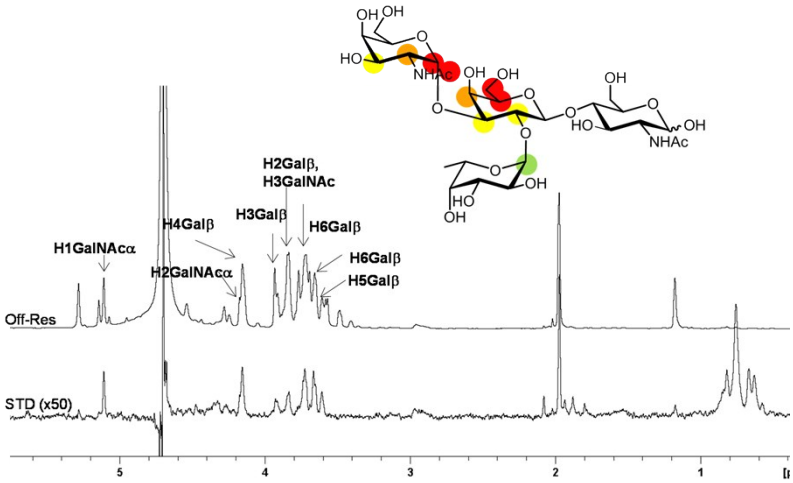

Fig S5. ^{1}H-STD-NMR experiment recorded at 298K for Gal-8C and A type II (**6**). The sample contained Gal-8C 50 µM and ligand **6** in 1.5 mM (ratio lectin:ligand = 1:30). **A**) Above: Determined epitope mapping A type II (**6**). Below: Off-resonance (irradiation at -30 ppm) and STD spectra (irradiation in the aliphatic region at 0.669 ppm) indicating the signals with the highest STD intensities.

2D-ROESY NMR

All 2D-ROESY experiments were acquired using Bruker AVANCE 2 800 MHz spectrometer equipped with cryoprobe. The 2D-ROESY spectra acquired for ligands **3** and **6** are reported here, and the most shifted protons are highlighted.

Interaction of ligands 3 and 6 with Gal-8N and Gal-8C.

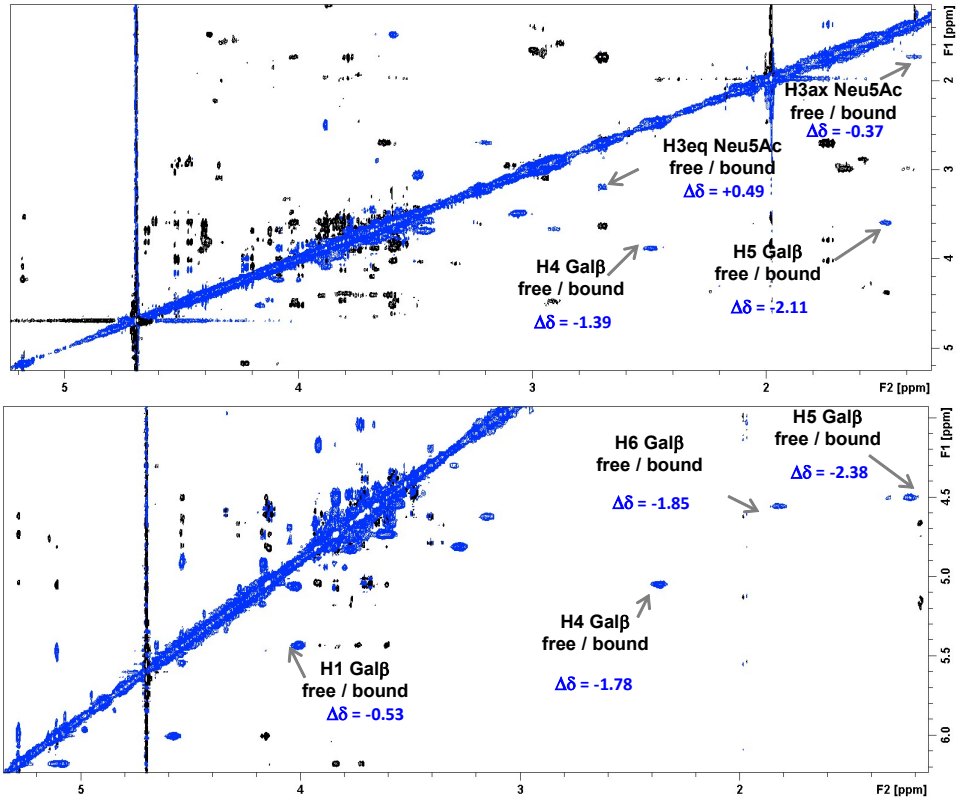

Fig S6. Above: 2D-ROESY-NMR for Gal-8N and 3-Sialyl-Galβ1-3GalNAc (**3**) at 298K. The sample contained Gal-8N 120 µM, **3** 1.2 mM (ratio lectin:ligand = 1:10). Below: 2D-trROESY-NMR for Gal-8C and A type II (**6**) at 298K.The sample contained Gal-8C 80 µM, **6** 0.8 mM (ratio lectin:ligand = 1:10). The signals with higher chemical shift perturbation were highlighted.

Interaction of ligands 3 and 6 with Gal-8FL.

A comparison with the data obtained for the interaction with the isolated N- and C-CRD is also included.

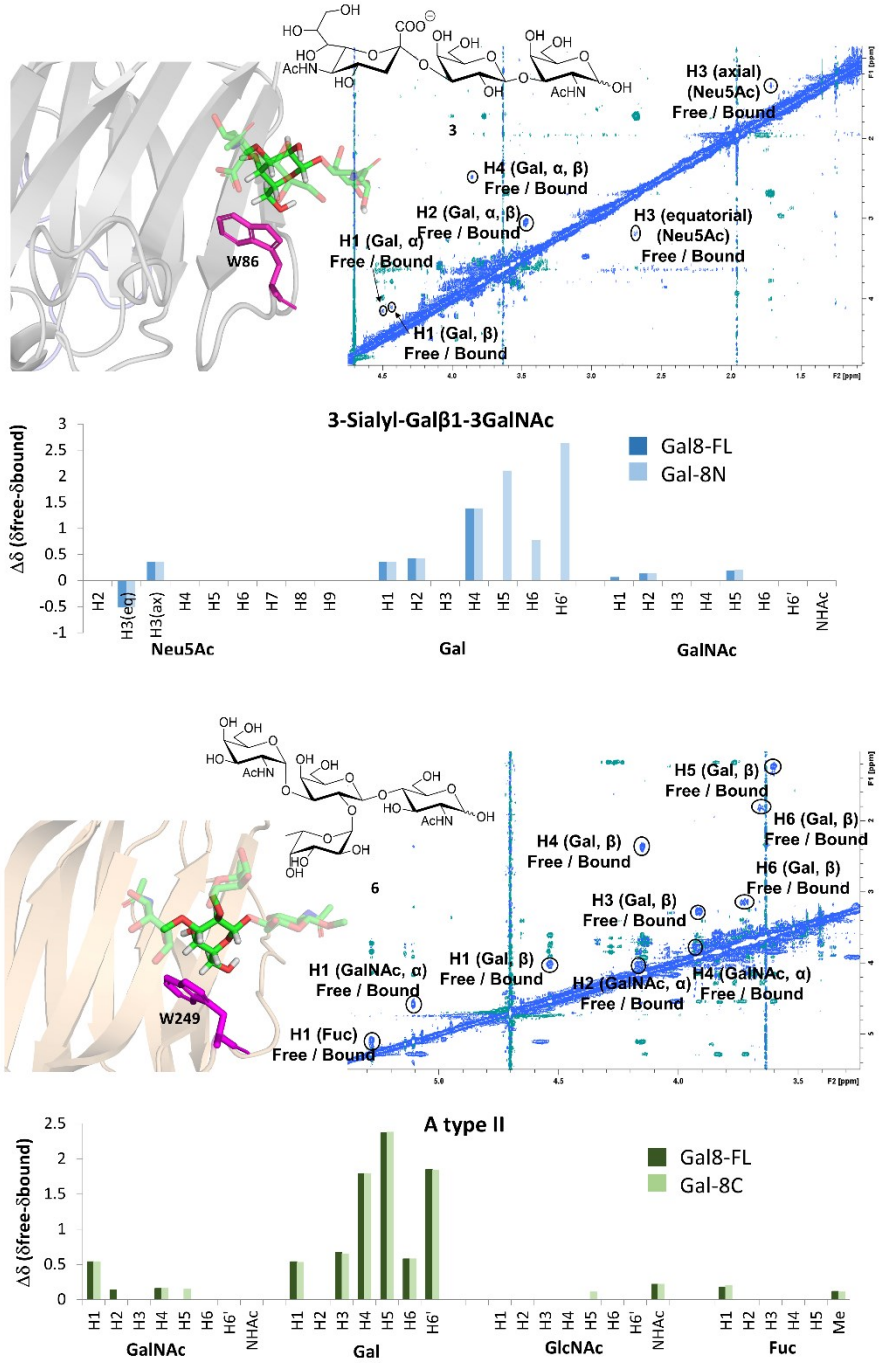

Fig S7. Above: 2D-ROESY-NMR for *h*Gal-8FL and 3-Sialyl-Galβ1-3GalNAc (**3**). The sample contained *h*Gal-8FL 100 µM, **3** 1.0 mM (ratio lectin:ligand = 1:10). The comparison of the chemical shift observed for ligand **3** in the presence of hGal-8FL and hGal8-N was also included. Below: 2D-trROESY-NMR for *h*Gal-8 and A type II (**6**).The sample contained *h*Ga8-FL 100 µM, **6** 0.8 mM (ratio lectin:ligand = 1:8). The comparison of chemical shift observed for ligand **6** in the presence of r hGal-8FL and hGal8-C was also included.

Superimposition of ^{15}N-HSQC spectra of Gal-8FL and their CRDs, Gal-8N and Gal-8C

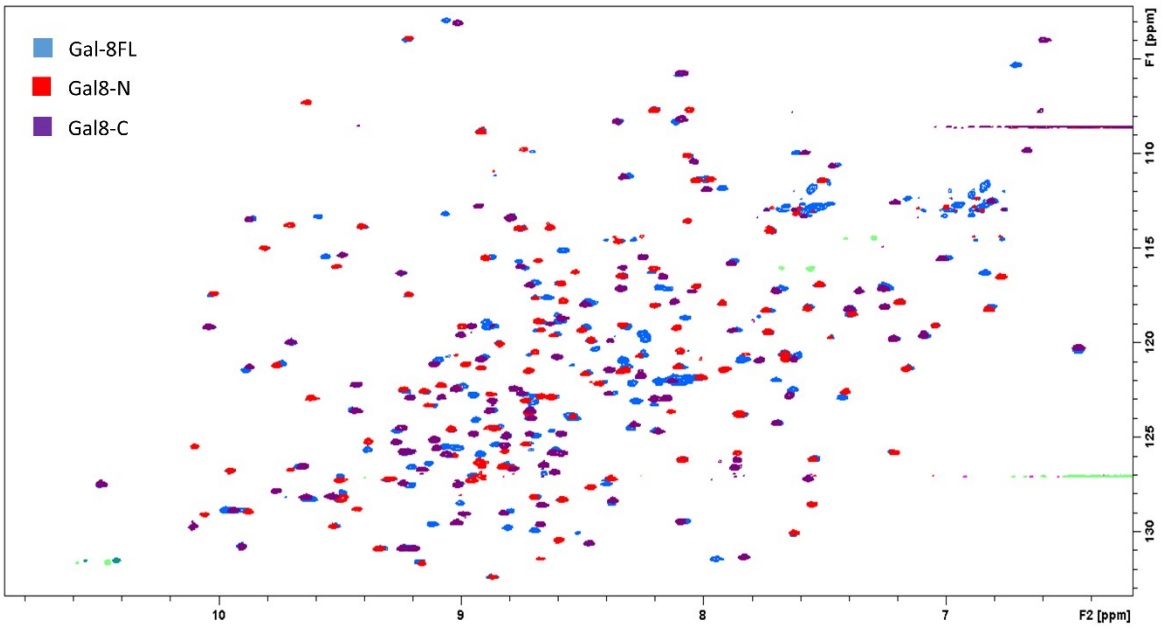

Fig S8. ^{15}N-HSQC spectra for Gal8-FL (blue) superimposed with Gal-8N (red) and Gal-8C (purple).

Chemical Shift Perturbation (CPS) analysis

The $\Delta\delta$ (ppm) = $[(\Delta\delta_H^2 + (0.14\cdot\Delta\delta_N)^2)/2]^{½}$ formula was employed to obtain the average ^{1}H and ^{15}N CSP of the NH groups of Gal-8FL backbone. All CSP were plotted with the most perturbed aminoacids being highlighted in the protein using a dark color if $\Delta\delta>2\sigma$ and a lighter version of the same color if $\Delta\delta>\sigma$.

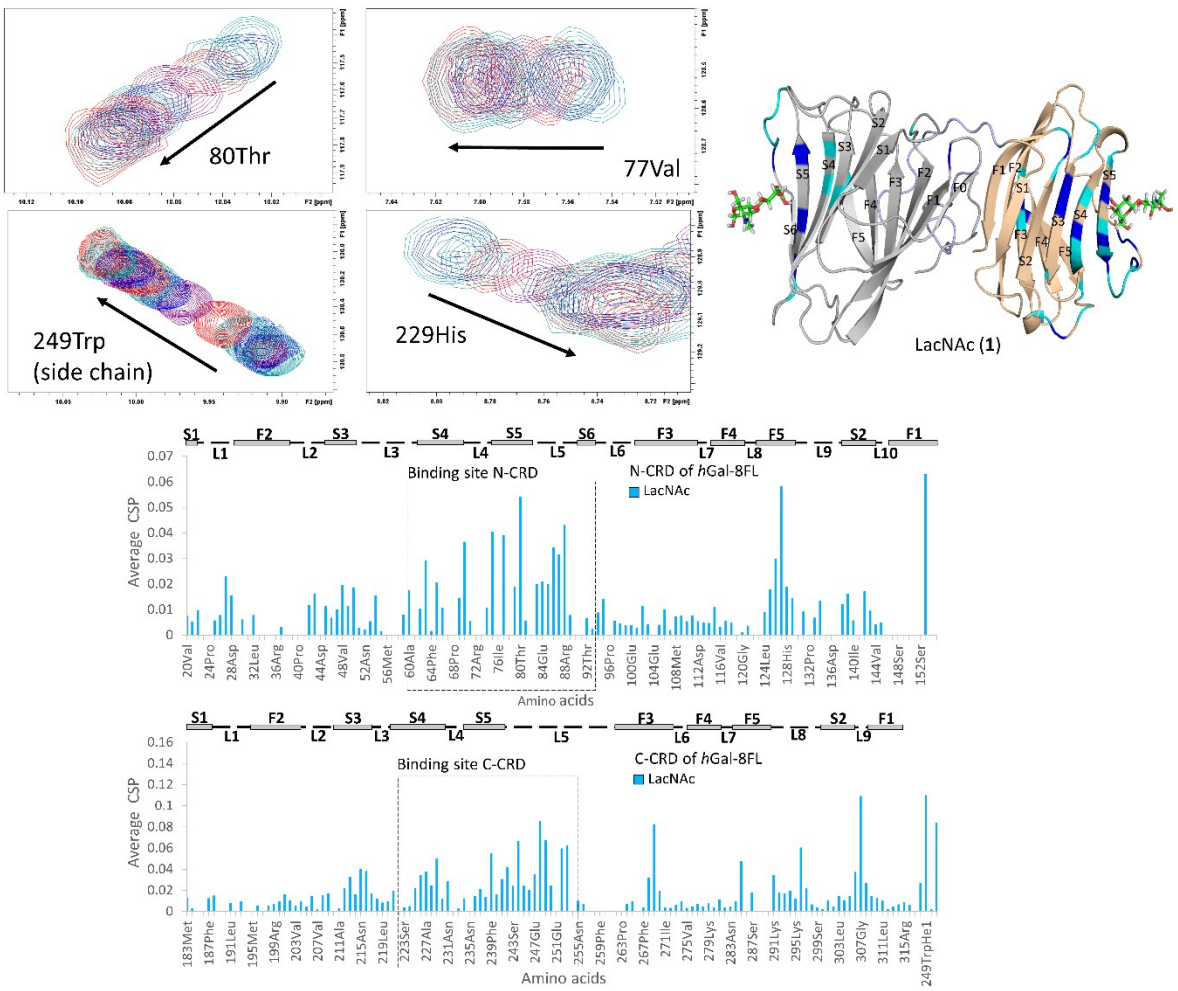

Fig. S9. Top left: expansions of ^{1}H-^{15}N HSQC spectra showing the CSP for a variety of residues of Gal-8FL in the N and C-CRD domains upon the adition of increasing amounts of LacNAc (**1**) up to saturation was reached. Top right: molecular model of the interaction of Gal-8FL and LacNAc (**1**) with the most perturbed aminoacids being highlighted in dark blue if $\Delta\delta>2\sigma$ and lighter blue if $\Delta\delta>\sigma$. Below: average CSP values for LacNAc (**1**) are detailed in blue.

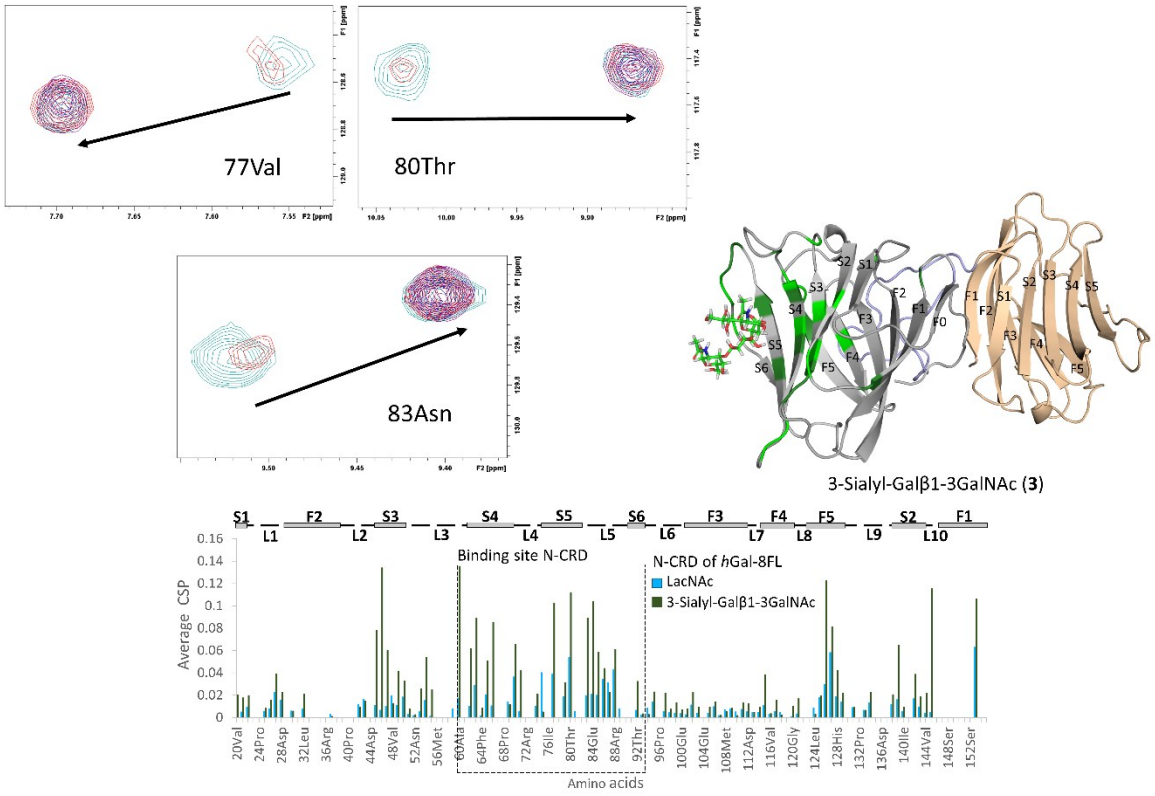

Fig. S10. Top left: expansions of ^{1}H-^{15}N HSQC spectra showing the CSP for a variety of residues of Gal-8FL (N-CRD domain) upon addition of different equivalents of 3-Sialyl-Galβ1-3GalNAc (**3**) up to saturation was reached. Top right: molecular model of the interaction of Gal-8FL and 3-Sialyl-Galβ1-3GalNAc (**3**) with the most perturbed aminoacids being highlighted in dark green if Δδ>2σ and lighter green if Δδ>σ. Below: average CSP values for 3-Sialyl-Galβ1-3GalNAc (**3**) are detailed in green in comparison with LacNAc (blue).

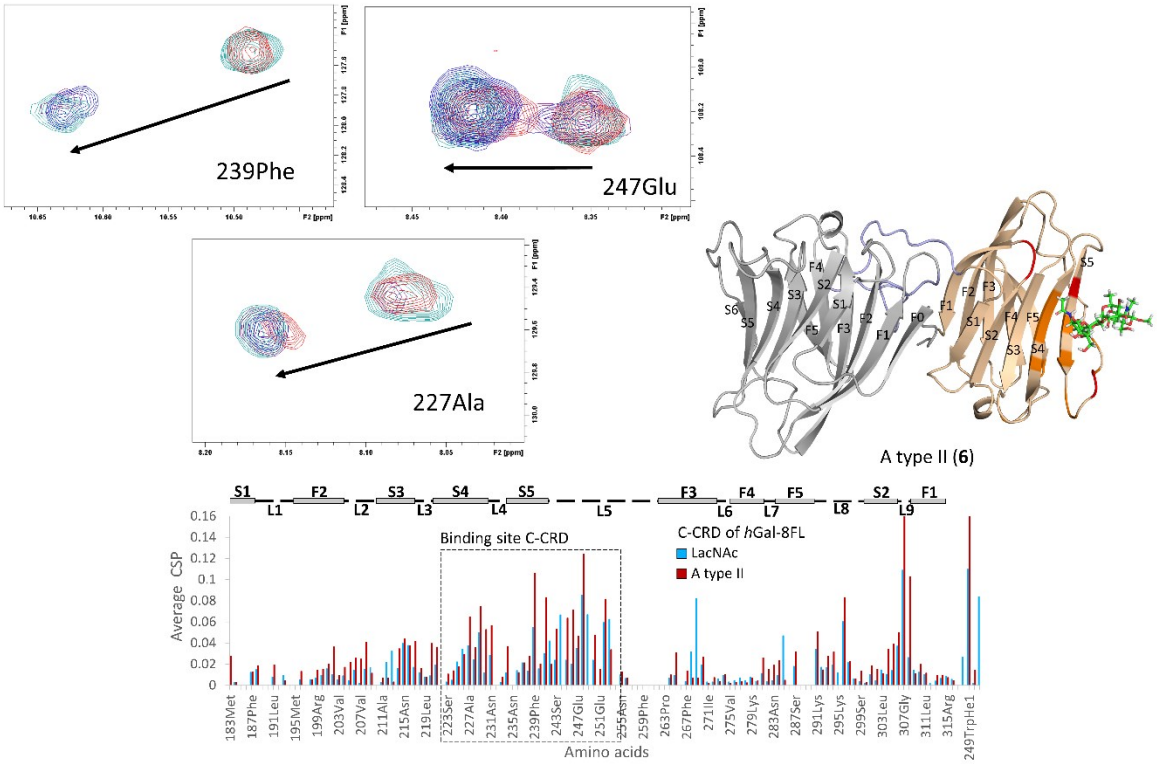

Fig. S11. Top left: expansions of ^{1}H-^{15}N HSQC spectra showing CSP for a variety of residues of Gal-8FL in (C-CRD domain) upon addition of different equivalents of A type II (**6**) up to saturation was reached. Top right: molecular model of the interaction of Gal-8FL and A type II (**6**) with the most perturbed aminoacids being highlighted in red if Δδ>2σ and light red if Δδ>σ. Below: average CSP values for A type II (**6**) are detailed in red in comparison with LacNAc (blue).

MOLECULAR MODELING AND MD SIMULATIONS

Model building

Full-length human galectin-8 was constructed from the crystallographic coordinates of the N- (PDB code: 4BMB; residues 1-150) and C-terminal (PDB code: 3OJB; residues 184-317) CRDs. The unresolved peptide linker (residues 151-183) was built in an extended conformation using the tleap module of Amber 18. The three fragments were manually assembled using PyMol and the resulting full-length structure was refined through MD simulations (see below).

Molecular Dynamics

Molecular dynamics (MD) simulations were run with the Amber 18 suite,[1,2] using the *ff14SB*[3] and *GLYCAM 06j-1*[4] force fields for the proteins and carbohydrate ligands, respectively. Binding histidine residues (H65 and H229) were modelled in their Nδ1-H tautomeric state (reside name HID in Amber).

Initial structures were neutralized with either Na^+ or Cl^- ions and set at the centre of a cubic TIP3P water[5] box with a buffering distance between solute and box of 10 Å. For each system, we followed a two-stage geometry optimization approach: the first stage minimizes only the positions of solvent molecules and ions, and the second stage is an unrestrained minimization of all the atoms in the simulation cell. The systems were then heated by incrementing the temperature from 0 to 300 K under a constant pressure of 1 atm and periodic boundary conditions. Harmonic restraints of 10 kcal mol^{-1} were applied to the solute, under the Andersen temperature coupling scheme.[6,7] The time step was kept at 1 fs during the heating stages, allowing potential inhomogeneities to self-adjust. Water molecules were treated with the SHAKE algorithm[8] such that the angle between the hydrogen atoms is kept fixed through the simulations. Long-range electrostatic effects were modelled using the particle mesh Ewald method.[9] An 8 Å cut-off was applied to Lennard-Jones interactions. Each system was equilibrated for 2 ns with a 2 fs time step at a constant volume and temperature of 300 K. Ten independent production trajectories were then run for additional 2.0 µs under the same simulation conditions, leading to accumulated simulation times of 20.0 µs for each system (*h*Gal-8, *h*Gal-8_N-term:LacNAc_C-term:LacNAc, *h*Gal-8_N-term:3-Sialyl-Galβ1-3GalNAc , *h*Gal-8_C-term:AtypeII, and *h*Gal-8_N-term:3-Sialyl-Galβ1-3GalNAc_C-term:AtypeII). For the complex used as a negative control (*h*Gal-8-_N-term:AtypeII_C-term:3-Sialyl-Galβ1-3GalNAc), five independent 1.0 µs production trajectories were run. Additionally, five 200 ns production trajectories were run for the isolated N- and C-terminal domains in complex with 3-Sialyl-Galβ1-3GalNAc and A type II respectively).

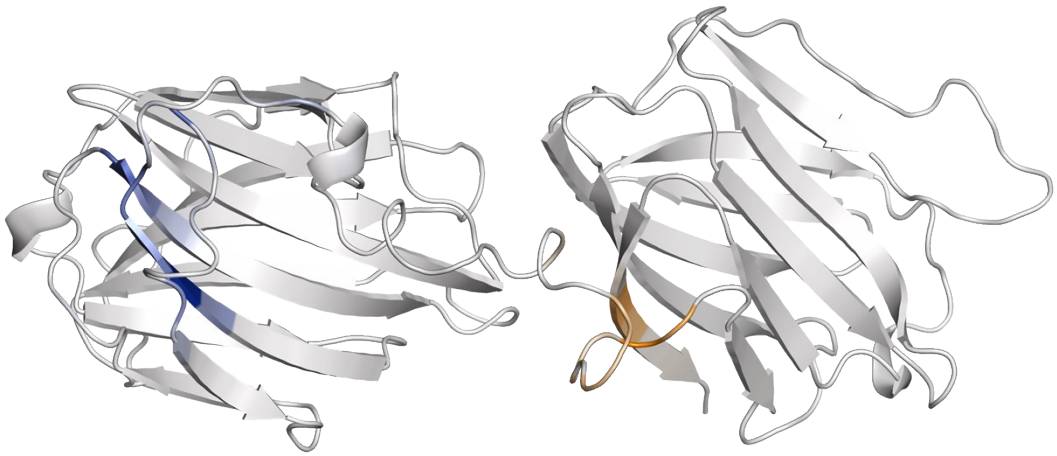

Fig. S12. Most frequent contacts between the peptide linker and N-terminal (in blue) and C-terminal (in orange) domains calculated throughout a 2 µs MD simulation of *apo* *h*Gal-8-FL. Contacts are considered if distance between any pair of atoms are closer than 4 Å.

Cluster search

In order to obtain the most representative structure for full-length *h*Gal-8, which was initially modelled in a fully extended conformation, all the production trajectories for the *apo* and bound systems with the ligands in their corresponding highest affinity binding sites were analysed together resulting in an accumulated simulation time of 100 μs. Conformations were sampled every 40 ns and clustered attending to the root-mean-square deviation (RMSD) of the N-terminal domain residues. The DBSCAN clustering algorithm[10] was used as implemented in the *cpptraj*[11] module of Amber 18. The distance cut-off between points for forming a cluster was set to 2 Å. At least 50 points were required to form a cluster and a total of 7 clusters were obtained (Table S1).

Table S1. Summary of cluster search results. Clusters are numbered starting from 0, being 0 the most populated. Next column indicates the number of frames in each cluster. *Frac* represents the size of cluster as a fraction of the total analysed trajectory. *AvgDist* is the average distance between points in the cluster. *Stdev* indicates the standard deviation of points in the cluster. *Centroid* is the frame in each cluster that has the lowest cumulative distance to every other point and *AvgCDist* is the average distance of this cluster to every other cluster.

Cluster	Frames	Frac	AvgDist	Stdev	Centroid	AvgCDist
0	66492	0.665	2.7	0.437	61554	2.212
1	1545	0.015	1.986	0.169	23546	2.835
2	1005	0.01	2.092	0.21	19409	2.441
3	928	0.009	2.203	0.215	58818	2.613
4	856	0.009	2.069	0.219	45774	2.885
5	689	0.007	2.178	0.252	47597	2.751
6	676	0.007	2.15	0.249	5463	2.811
7	565	0.006	2.036	0.142	59696	2.387
8	480	0.005	2.043	0.197	39879	2.895

Allosteric network analysis

Proteins can be treated as a four-dimensional network of discrete nodes (amino acids) interconnected through space and time. The result of this crosstalk between the constituting amino acids, which can be largely affected by environmental factors (solvent, ionic strength, temperature, substrate binding, etc.), defines the structure, dynamics and ultimately the properties of a given protein. Although usually the most effective communication between these nodes takes place through direct covalent or noncovalent interactions, identification of allosteric pathways between pairs of residues that are not directly linked has been investigated using dynamical network and correlated residues analysis. The allosteric communication between the active sites and distant regions of the N- and C- terminal domains of hGal-8 was analyzed through molecular dynamics simulations. From these simulations, optimal and suboptimal pathways for dynamic correlation between binding residues and any other

amino acid in the protein were traced (Figure S13) using the Weighted Implementation of Suboptimal Paths (WISP) algorithm.[12]

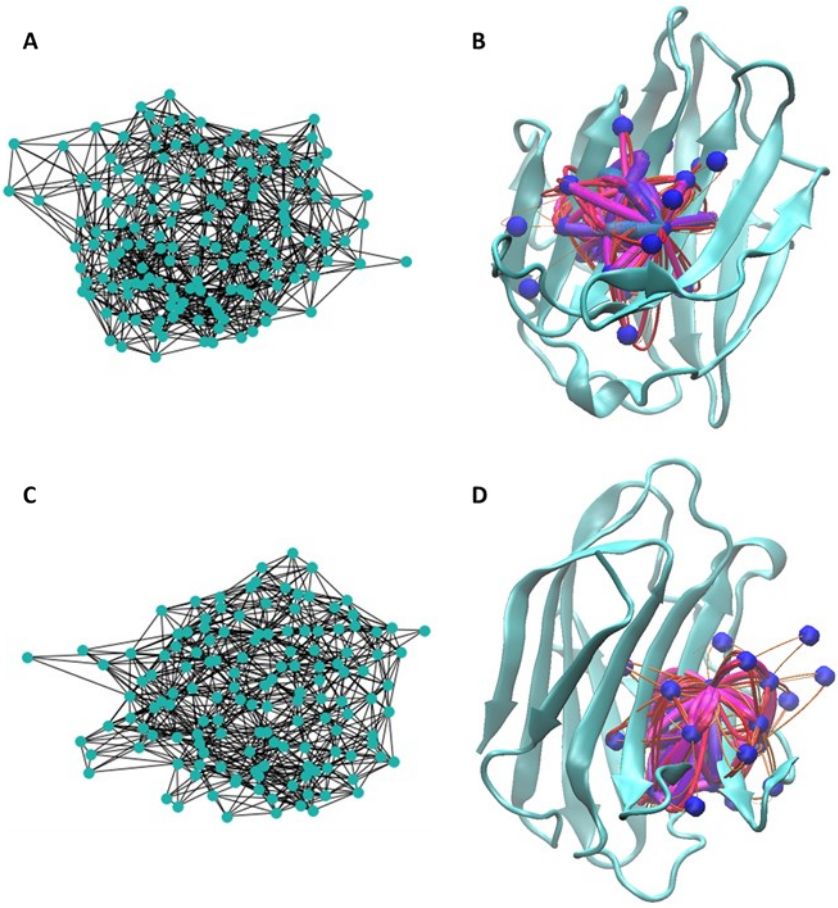

Fig S13. Dynamic correlation network representation calculated from MD simulations for *h*Gal-8 N-terminal domain (**A**) and *h*Gal-8 C-terminal domain (**C**); nodes represent the side chain residues center of mass and edges are defined by a metric quantifying the interdependence among nodes. Examples of 100 optimal and suboptimal pathways based on correlated motions for *h*Gal-8 N-terminal domain (**B**) and *h*Gal-8 C-terminal domain (**D**) between selected pairs of residues (HID65-ILE140, HID46-TYR107 respectively).

First, a correlation matrix (C_{ij}) is generated from 1,000 snapshots extracted every 200 ps from a converged MD trajectory, by calculating the correlation motion among node-node pairs with Eq. 1. In our model, nodes are defined by the side-chain residue center of mass, and two nodes are considered to be in contact if the mean distance between them along the MD simulation is 6 Å or less. The length of the edges connecting these nodes quantifies the degree of dynamic communication between pairs of connected nodes as defined in Eq. 2. This pathway length is inversely proportional to the correlation motion between nodes, meaning that shorter w_{ij} values indicate tightly correlated or anticorrelated nodes, whereas larger values indicate less correlated nodes.

$$C_{ij} = \frac{\langle \Delta\vec{r}_i(t) \cdot \Delta\vec{r}_j(t) \rangle}{\sqrt{\langle \Delta\vec{r}_i(t)^2 \rangle \langle \Delta\vec{r}_j(t)^2 \rangle}} \qquad \text{Eq.1}$$

$$w_{ij} = -\log(|C_{ij}|) \qquad \text{Eq.2}$$

Then, Dijkstra's algorithm is used to generate all force-node paths, finding the shortest (i.e. optimal) path. To identify not only the optimal but also suboptimal pathways, WISP employs a bidirectional search. Suboptimal pathways are defined as those closest in length to the optimal one, but not including it. The available code rapidly calculates both optimal and suboptimal communication pathways between two user-specified residues of a protein. For both N- and C-terminal *h*Gal-8 domains, 100 pathways were calculated between selected binding site resides (H46 and W66) and all the other residues of the protein. These paths were calculated for the *bound* forms with two different ligands (3-Sialyl-Galβ1-3GalNAc and A type II in complex with *h*Gal-8 N- and C-terminal domains respectively).

The so-called length of these calculated pathways can be mapped and color-coded onto the protein structure to obtain a visual representation of the internal correlated motions (Figure S14 **A** and **C**). Similarly, the frequency at which a given amino acid is involved in the calculated allosteric pathways, can be represented to easily identify which residues operate as critical nodes to relay dynamic information inside the protein (Figure S14 **B** and **D**).

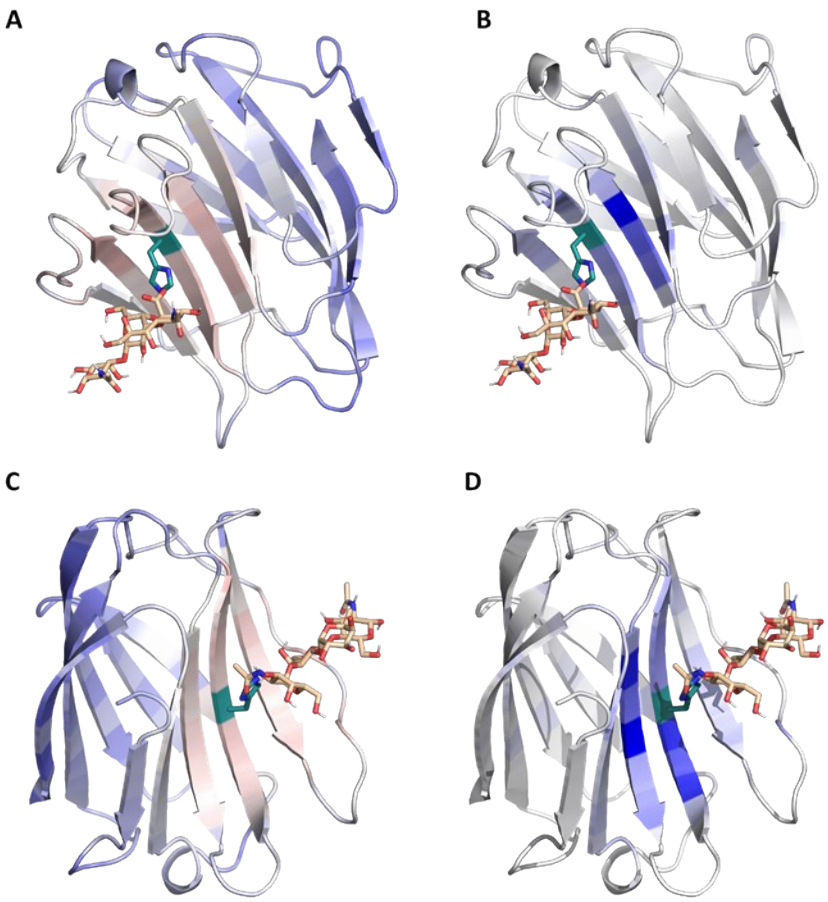

Fig S14. Dynamic correlation network representation calculated from MD simulations for *h*Gal-8 N-terminal domain (**A** and **B**) and *h*Gal-8 C-terminal domain (**C** and **D**). The allosteric pathways determined from selected residues (shown as turquoise sticks) and the rest of the protein are color-coded from red (short/efficient) to blue (long/inefficient) (**A** and **C**). For each system, the nodes (i.e. residues) colored in blue in figures **B** and **D** are those appearing most frequently in all the 100 calculated optimal and suboptimal allosteric pathways.

Isothermal titration calorimetry (ITC)

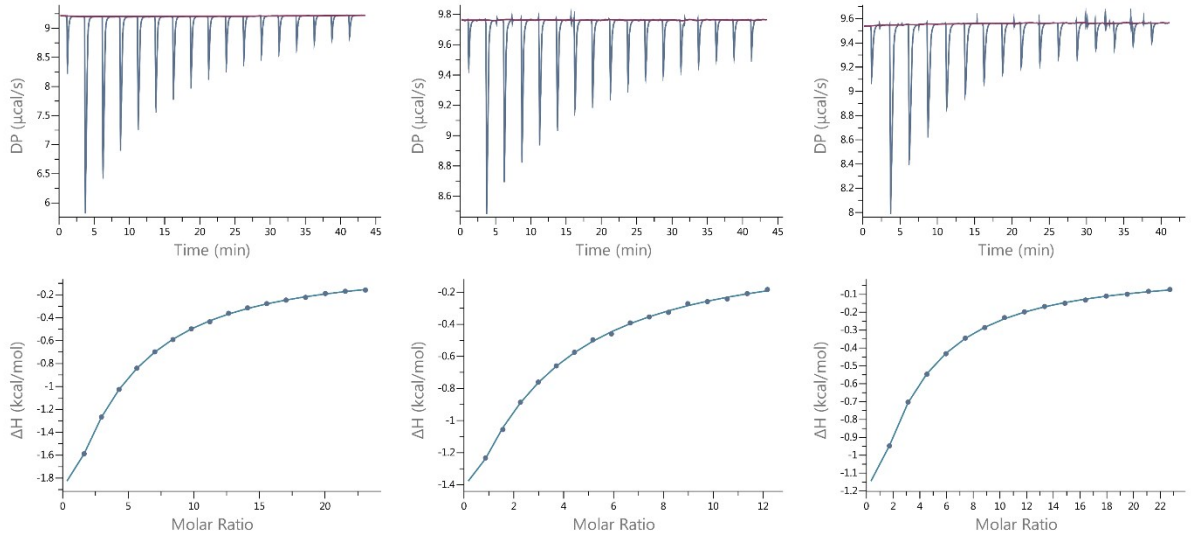

LacNAc(**1**):Gal8-FL LacNAc(**1**):Gal-8N LacNAc(**1**):Gal-8C

Fig S15. Example of titration profiles obtained from the titrations of Gal-8FL, Gal8-N, Gal8-C with LacNAc **1**. Above:depiction of the titration representing µcal/sec dispersed as a function of time. Below: binding isotherm of the calorimetric titration (enthalpy (kcal/mol) is plotted against the molar ratio of Gal-8:ligand in the cell).

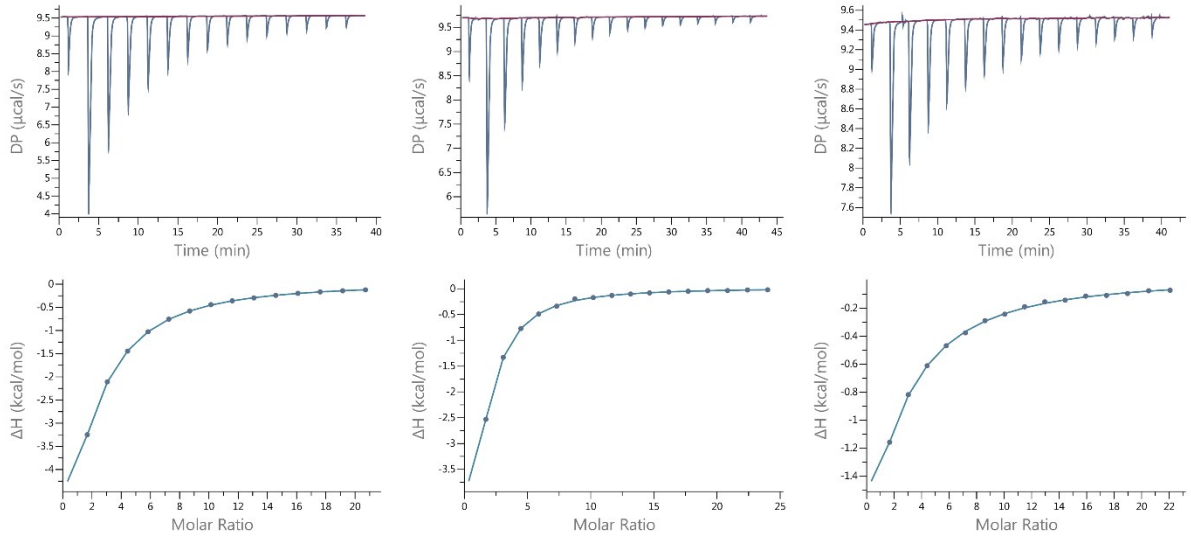

Galβ1-3GalNAc (**2**):Gal8-FL Galβ1-3GalNAc (**2**):Gal-8N Galβ1-3GalNAc (**2**):Gal-8C

Fig S16. Example of titration profiles obtained from the titrations of Gal-8FL, Gal8-N, Gal8-C with Galβ1-3GalNAc **2**. Above:depiction of the titration representing µcal/sec dispersed as a function of time. Below: binding isotherm of the calorimetric titration (enthalpy (kcal/mol) is plotted against the molar ratio of Gal-8:ligand in the cell).

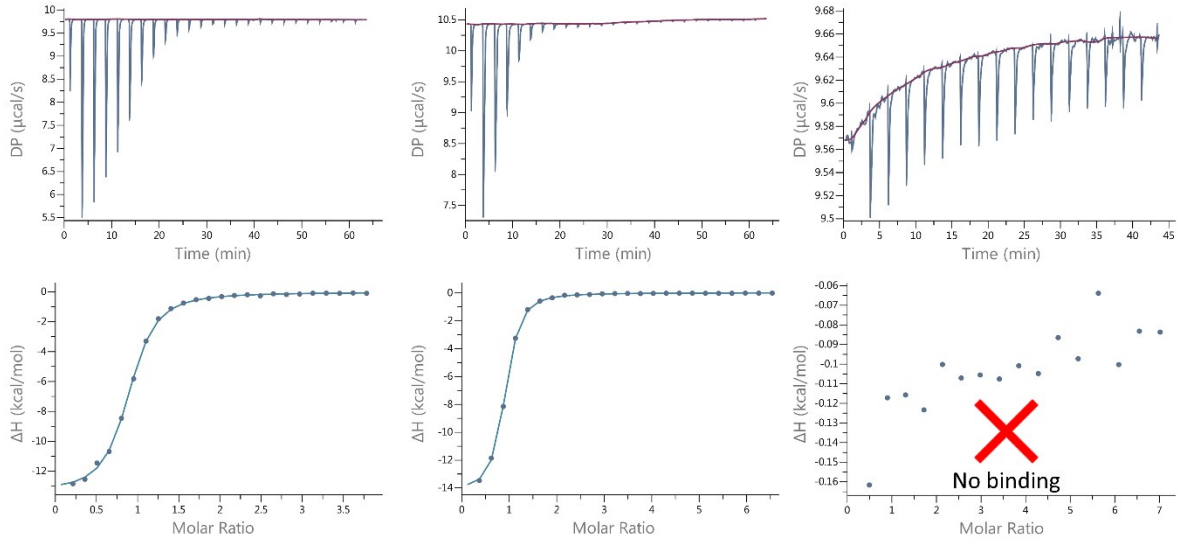

3-Sialyl-Galβ1-3GalNAc (**3**):Gal8-FL 3-Sialyl-Galβ1-3GalNAc (**3**):Gal-8N 3-Sialyl-Galβ1-3GalNAc (**3**):Gal-8C

Figure S17. Example of titration profiles obtained from the titrations of Gal-8FL, Gal8-N, Gal8-C with 3-Sialyl-Galβ1-3GalNAc **3**. Above:depiction of the titration representing µcal/sec dispersed as a function of time. Below: binding isotherm of the calorimetric titration (enthalpy (kcal/mol) is plotted against the molar ratio of Gal-8:ligand in the cell).

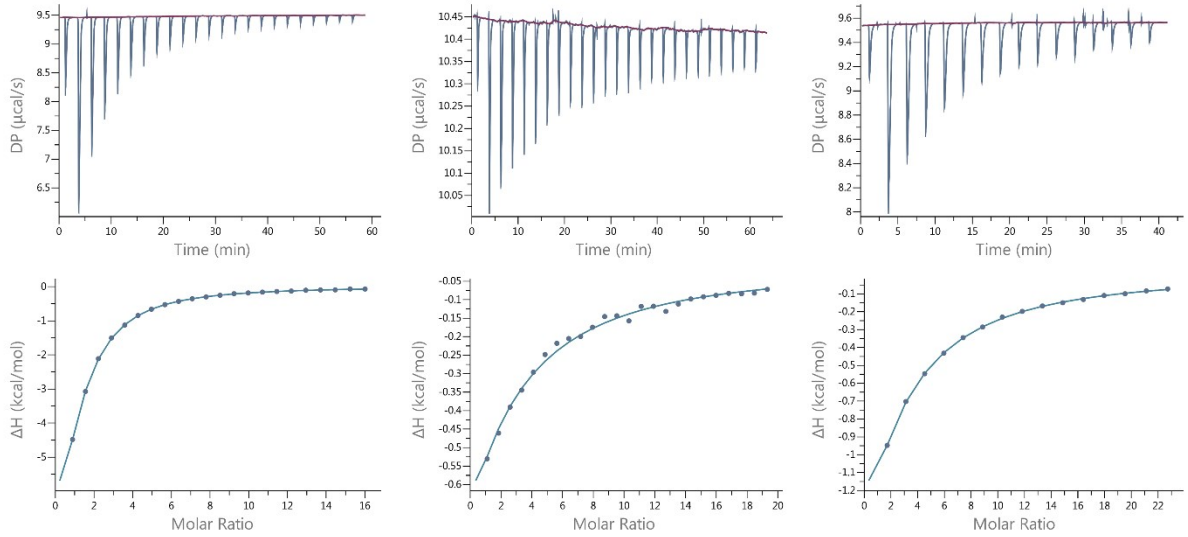

Galili (**4**):Gal8-FL Galili (**4**):Gal-8N Galili (**4**):Gal-8C

Fig S18. Example of titration profiles obtained from the titrations of Gal-8FL, Gal8-N, Gal8-C with Galili **4**. Above:depiction of the titration representing µcal/sec dispersed as a function of time. Below: binding isotherm of the calorimetric titration (enthalpy (kcal/mol) is plotted against the molar ratio of Gal-8:ligand in the cell).

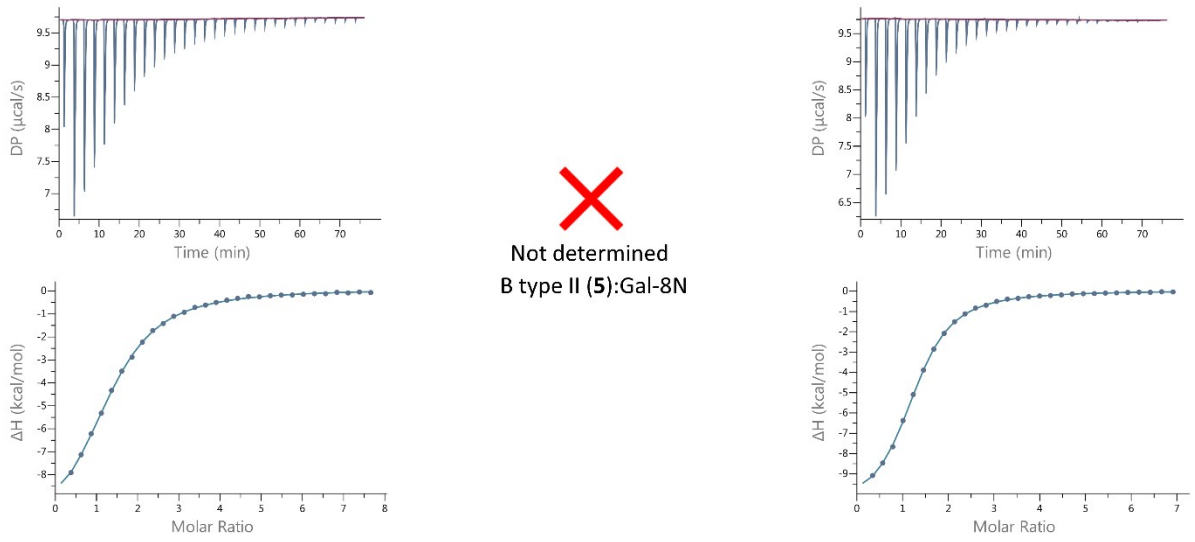

Fig S19. Example of titration profiles obtained from the titrations of Gal-8FL, Gal8-C with B type II **5** (No experiments were acquired for B type II:Gal-8N as no binding was already observed for A type II:Gal-8N. Above:depiction of the titration representing µcal/sec dispersed as a function of time. Below: binding isotherm of the calorimetric titration (enthalpy (kcal/mol) is plotted against the molar ratio of Gal-8:ligand in the cell).

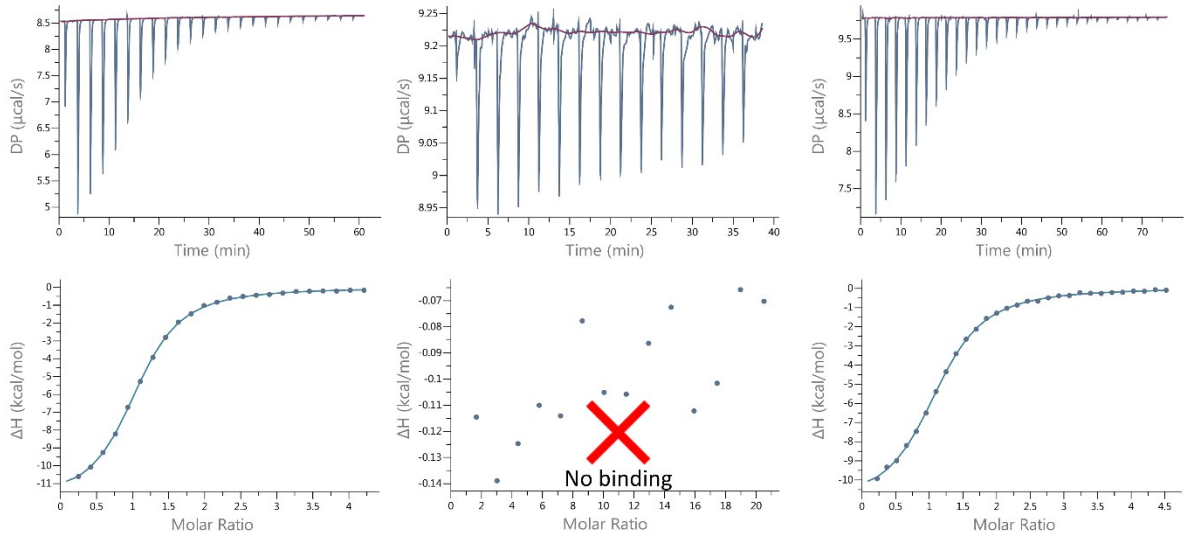

Fig S20. Example of titration profiles obtained from the titrations of Gal-8FL, Gal8-N, Gal8-C with A type II **6**. Above:depiction of the titration representing µcal/sec dispersed as a function of time. Below: binding isotherm of the calorimetric titration (enthalpy (kcal/mol) is plotted against the molar ratio of Gal-8:ligand in the cell).

ITC ligand competition experiments

In order to prove that the CRDs were not affected by the presence of ligands in the opposite CRD, each domain was preloaded with its respective ligand (10 equivalents of 3-Sialyl- Galβ1-3GalNAc (**3**) for N-CRD and 8 equivalents of A type II (**6**) for C-CRD) and the thermodynamic data was acquired with ligands **6** and **3**, respectively. (Figure S21).

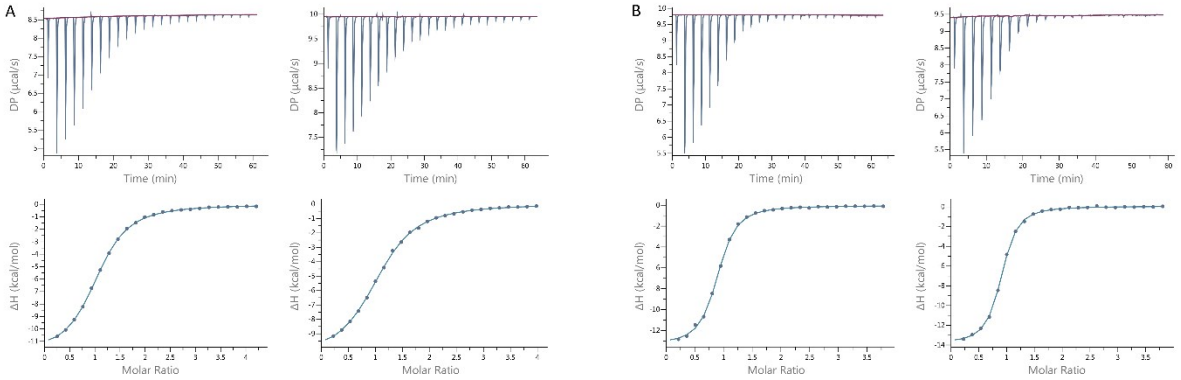

Fig S21. A) Energetic profile of the binding of A type II (**6**) to the C-CRD of Gal-8FL (left) compared to the binding of A type II (**6**) to the C-CRD in the presence of 3-Sialyl-Galβ1-3GalNAc (**3**) in the N-CRD of Gal-8FL (right). B) Energetic profile of the binding of 3-Sialyl-Galβ1-3GalNAc (**3**) to the N-CRD of Gal-8FL (left) compared to the binding of 3-Sialyl-Galβ1-3GalNAc (**3**) to the N-CRD in the presence of A type II (**6**) in the C-CRD of Gal-8FL.

Table S2. K_D and thermodynamics parameters for the interactions of ligands **1**-**6** with Gal-8FL, Gal-8 N and Gal-8C , as determined by ITC. The thermodynamic parameters for the binding of ligands **3** and **6** to Gal-8FL glycan pre-loaded species (runs in which the opposite CRD was preloaded with ligands **6** and **3**) are indicated in parenthesis.

		LacNAc (**1**)	Galβ1-3GalNAc (**2**)	3-Sialyl-Galβ1-3GalNAc (**3**)	Galili (**4**)	B type II (**5**)	A type II (**6**)
Gal8-FL	K_D (μM)	804±2	229±24	4.3±0.4 (3.0±0.2)	165±4/68±2	36.7±0.6	12±1 (17±1)
	ΔG (kcal/mol)	-4.22±0.01	-4.96±0.06	-7.33±0.05 (-7.52±0.03)	5.16±0.4/ -5.68±0.01	-6.05±0.01	-6.71±1 (-6.50±0.04)
	ΔH (kcal/ mol)	-	-	-13.5±0.1 (-14.1±0.1)	-	-10.9±0.2	-11.9±0.2 (-10.7±0.4)
	-TΔS (kcal/mol)	-	-	6.2±0.2 (6.6±0.2)	-	4.8±0.2	5.1±0.1 (4.20±0.01)
	N	2	2	0.92±0.06 (0.77±0.08)	1/2	1.36±0.02	1.09±0.05 (1.07±0.02)
Gal-8N	K_D (μM)	621±43	186±5	2.2±0.1	444±34	-	-
	ΔG (kcal/mol)	-4.38±0.04	-5.08±0.01	-7.72±0.04	-4.57±0.04	-	-
	ΔH (kcal/ mol)	-	-	-13±1	-	-	-
	-TΔS (kcal/mol)	-	-	5±1	-	-	-
	N	1	1	0.90±0.09	1	-	-
Gal-8C	K_D (μM)	844±135	348±216	-	115.5±0.5	18.4±0.1	13.45±0.05
	ΔG (kcal/mol)	-4.02±0.09	-4.9±0.3	-	-5.37±0.01	-6.46±0.01	-6.65±0.01
	ΔH (kcal/ mol)	-	-	-	-	-10.7±0.1	-11.2±0.1
	-TΔS (kcal/mol)	-	-	-	-	4.3±0.1	4.6±0.1
	N	1	1	-	1	1.26±0.03	1.13±0.01

References

1. D. A. Case, *et al.* Amber 2018; 2018. *University of California, San Francisco* (2018).
2. T. S. Lee, *J. Chem. Inf. Model.,* 2018, **58***,* 2043.
3. J. A. Maier, *et al., J. Chem. Theory Comput.*, 2015, **11**, 3696.
4. K. N. Kirschner, *et al.*, *J. Comput. Chem.*, 2008, 29, 622.
5. W. L. Jorgensen, J. Chandrasekhar, J. D. Madura, R. W. Impey, and M. L. Klein, *J. Chem. Phys.,* 1983, **79**, 926.
6. H. C. Andersen, *J. Chem. Phys.,* 1980, **72**, 2384.
7. T. A. Andrea, W. C. Swope, and H. C. Andersen, *J. Chem. Phys.,* 1983, **79**, 4576.
8. S. Miyamoto, and P. A. Kollman, *J. Comput. Chem.,* 1992, **13**, 952.
9. T. Darden, D. York, and L. Pedersen, *J. Chem. Phys.*, 1993, **98**, 10089.
10. M. Ester, H.-P. Kriegel, J. Sander, and X. A. Xu, *Proceedings of the 2nd International Conference on Knowledge Discovery and Data Mining*, 1996, 226.
11. D. R. Roe, and T. E. Cheatham, *J. Chem. Theory Comput.,* 2013, **9**, 3084.
12. A. T. Van Wart, J. Durrant, L. Votapka, and R. E. Amaro, *J. Chem. Theory Comput.,* 2014, **10**, 511.